Title

Global Activity Search Uncovers Reaction Induced Concomitant Catalyst Restructuring for Alkane Dissociation on Model Pt Catalysts

Permalink

https://escholarship.org/uc/item/6pv7j9bf

Journal

ACS Catalysis, 11(3)

ISSN

2155-5435

Authors

Sun, Geng
Fuller, Jack T
Alexandrova, Anastassia N
et al.

Publication Date

2021-02-05

DOI

10.1021/acscatal.0c05421

Supplemental Material

https://escholarship.org/uc/item/6pv7j9bf#supplemental

Global Activity Search Uncovers Reaction Induced Concomitant Catalyst Restructuring for Alkane Dissociation on Model Pt Catalysts

Geng Sun[1], Jack T. Fuller III,[2] Anastassia N. Alexandrova[2,3]*, Philippe Sautet [1,2,3]*

[1]Department of Chemical and Biomolecular Engineering, University of California, Los Angeles, Los Angeles, California 90095, United States

[2]Department of Chemistry and Biochemistry, University of California, Los Angeles, Los Angeles, California 90095, United States

[3]California Nano Systems Institute, Los Angeles, California 90095-1569, United States

*Corresponding authors

ana@chem.ucla.edu

sautet@ucla.edu

Abstract

Although there are evidences that catalytic active sites can restructure under reaction conditions, their optimal reconstruction to provide the lowest activation barrier is still unclear. Here we show, with methane activation on supported Pt clusters and by an explicit sampling of cluster configurations at the transition state, that important restructuring is required to reach the most active transition state. The capability of the cluster to reconstruct, simultaneously with the C-H dissociation, is a key aspect for catalytic activity. We underline two types of reconstructions, concomitant or independent, depending on whether they emerge in or off the course of reactive trajectories. The concomitant reconstructions depict the significant rearrangement of the catalyst itself as part of the reaction coordinate, and play critical roles in the most competitive pathways. The best active sites can be only found in the course of the reactive trajectories and not from the equilibrium geometry prior the reaction.

1 Introduction

There is more and more evidence that surface sites at heterogeneous catalysts are not static at the atomic scale but instead present ample and dynamic restructuring phenomena in reaction conditions.[1-4] In addition, low energy metastable configurations can be accessible and feature enhanced activity.[5-7] This sets a strong challenge for realistic and accurate modelling of heterogeneous catalytic process. One key question is to determine "how" a catalytic site can optimally restructure to provide the lowest activation barrier in link with the measured catalytic activity. The question is non-trivial since catalytic sites usually have a large number of degrees of freedom. As a result, most studies still assume that the catalyst during reaction is static and only undergoes a limited local relaxation. Here we propose a method for the global search of transition states for a catalytic reaction with a detailed sampling of configurations of the catalytic active site. We invert the order in the reaction profile construction, first determining catalyst structures that provide low energy transition states, then connecting these saddle points to the locally stable reactant state. The approach uncovers optimal restructuring events for the catalytic site that we could not obtain by standard reaction pathways searches, starting from the global minimum or from metastable structures of the catalytic site, underlining the key importance of sampling catalyst configurations at the catalytic reaction transition state. In addition, not one but a large number of reaction channels contribute to the catalytic reaction rates.

The catalyst chosen to illustrate our approach consists in supported sub-nanometer metal clusters, which are not only model catalytic systems for academic studies,[5, 8-9] but also represent a class of practical catalytic materials used in many important industrial processes.[8, 10-21] For example, sub-nanometer Pt particles supported on γ-alumina is a widely used and stable catalyst for naphtha reforming into high-octane gasoline, involving dehydrogenation and hydrogenolysis reactions, and also more recently for alkane dehydrogenation, both reactions taking place at high temperature (500-600 °C).[22-24] The preparation produces Pt clusters of size ~0.9 nm (i.e. about 10 Pt atoms). As a general model, we consider here alkane dehydrogenation reactions on γ-Al_2O_3(100) supported Pt_7 and Pt_8 clusters in realistic conditions, i.e. at 600 °C and under a H_2

pressure of 0.1 bar. The cluster thus bears a coverage of H atoms, which is fully sampled. We focus on the first C-H bond dissociation of the alkane, and take methane as a model for that first step.

Nanoclusters do not appear as only a static global minimum (GM) geometry, but can undergo isomerization to metastable structures corresponding to different minima of the free energy surface through rare events characterized by low energy transition states (TS). [25-27] At the high temperature used in catalysis, such isomerization is fast, enabling to access metastable configurations with distinct electronic structures which might dominate the catalytic reactivities.[5, 27-29] However, if the ensemble nature of low energy isomers and the presence of dynamic reconstructions[24,25] have been shown for clusters, the nature of the catalytic active site on each isomer and the relation between the ensemble of cluster isomers and the rate of the catalytic reaction are still mostly unknown. Indeed, considering the large number of low energy configurations[5, 29-30] and the low-symmetry of the clusters, the explicit exploration of the catalytic reactivity on fluxional cluster catalysts is a great theoretical and computational challenge. A common approach used in the literature is to first find the ensemble of stable clusters by either global optimizations or molecular dynamics simulations, and then to explore the transition state (TS) structures on several stable cluster configurations. We will show that such as stepwise method can lead to incorrect results. When the cluster is highly flexible, its significant structural rearrangement might take place with the reaction, and even couple to it dynamically.[31] Then, it is possible that reaction paths involving such catalyst reorganizations are more catalytically active than the more traditional pathways involving just the reagent activity on a static structure of the catalyst. However, when calculating reaction profiles on cluster catalysts, such reorganizations beyond small adjustment of the cluster geometry are not specifically sought, and thus, not found. The most critical fundamental question is how much reaction-reconstruction interaction contributes to the global activity in nanocatalysis in a realistic mixture of catalyst isomers with large numbers of degrees of freedom. Therefore, our goal goes beyond the simple recognition of any single type of reaction mechanism initialized from picking one configuration.

Our new method, dubbed Global Activity Sampling (GAS) directly and globally optimizes the configuration of the supported cluster corresponding to the TS for the catalytic reaction without requiring a prior knowledge on stable cluster structures, hence overcoming the potential limitations of the aforementioned stepwise method. In GAS, grand canonical perturbations[32-36] and Basin

Hopping moves enable the method to explore TSs that are associated with clusters including various adsorbed species at chosen reaction condition, and their various isomers. When the configurations minimizing the TS are found, the precursor structures of the clusters that connect to these TSs can be obtained in a second step. The approach uncovers critical reconstruction phenomena which only take place in the course of reactive trajectory, and are unlikely to be found following the standard approach.

2 Results and discussions

2.1 Sampling activity space for C-H bond dissociation in methane

The key design characteristic of the GAS method is that it determines **configurations of the catalytic system** that produce minimal free energy transition state (TS) for a considered catalytic reaction, hence directly sampling the activity space (See Figure 1 and section S1.1). The target function of GAS is the free energies of the TS of the rate-determining step, instead of the stability of the cluster catalyst itself (see Method section). GAS consists of a series of local steps determining the TS first before optimizing the reactant state. Atomic positions and hydrogen coverage of TS structures are modified by Monte-Carlo steps following the selected reaction condition.[32-36]. Some technical aspects such as TS estimation[37-39] are also used to save CPU time and more details can be found in the SI Section 1.

The approach is used to explore the TS for C-H bond dissociation in methane, and sampling cluster configuration and H coverage of the two considered supported clusters, Pt_7 and Pt_8. It generates an ensemble of reaction pathways presenting low free energy TSs and hence highest catalytic activity for methane dissociation. Each structure in this TS ensemble is linked to an entry configuration (EC), being a local minimum of the H covered cluster in the absence of methane, that can be optimized from the TS following the gradient along the reaction coordinate (Figure 1). A reaction pathway is uniquely defined as the pair of EC-TS structures. Although we did not look in detail into the isomerization pathways between cluster minima, the isomerization kinetics is expected to be reasonably fast compared to methane activation (see further discussion in section 2.3 and refs [30, 40]); hence the population of different ECs are being treated as an equilibrium. In consequence, the optimal reaction pathway corresponds to the lowest free energy TS, which is globally optimized during the GAS explorations.

Biased molecular dynamics approaches, such as metadynamics, have been used in the literature to study reactions on a high dimensional potential energy surface.[41-42]. Such methods were for example applied to CO oxidation on Pt(111)[43], or CO_2 hydrogenation on Cu/ZnO catalyst models.[44] However only a few collective variables (generally smaller than 3) can be used, focusing the sampling of the surface species, while degrees of freedom associated with the catalytic site are not efficiently sampled. The proposed GAS method provides some advantages over such metadynamics simulations for heterogeneous catalytic reactions. First, all the degrees of freedoms of the clusters are relaxed and sampled in GAS. Second, the GAS method samples the catalyst with varying hydrogen coverage in a grand canonical condition. Constructing a constant H_2 reservoir is challenging in molecular dynamics simulation because a very large simulation box has to be used to accommodate the sufficient number of H_2 molecules. Finally, the number of required force/energy evaluations in GAS is also appealingly small compared with molecular dynamics simulations (details are discussed in SI section 1.2).
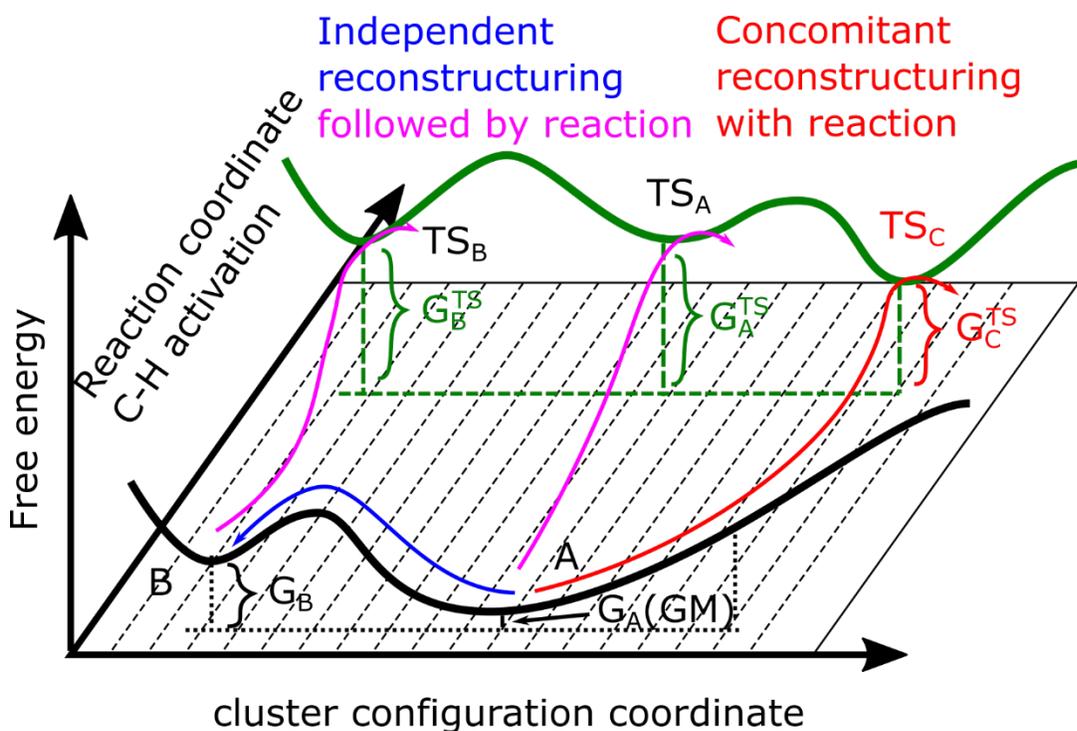

Figure 1: A schematic illustration of the GAS method. The green line shows the potential energy surface of the clusters implicitly constrained to stay at a transition state for methane C-H dissociation, which is explored first by GAS. The black line shows the potential energy surface of the clusters. In contrast to the conventional way in which local minima A and B are explored first, the GAS method starts by exploring cluster configurations corresponding to low energy TSs (TS$_A$, TS$_B$, TS$_C$) and find the local minima (A and B) afterwards. Therefore, GAS directly and globally optimizes G^{TS} without requiring the prior knowledge of the cluster geometries.

The GAS method produced 504 (resp. 470) unique EC-TS pairs corresponding to reaction pathways for C-H dissociation using Pt_7 (resp. Pt_8) on γ-Al_2O_3. Those with lowest energy TSs are depicted in Figure 2(a) (resp. Figure 2(b)) in which the TSs have been confirmed by vibrational analysis. The ordinate represents the TS energy being an indicator of reactivity, while the abscissa shows the free energy of the corresponding EC with respect to the GM of the H covered clusters. Each EC may initialize several reaction pathways, either occurring on different Pt sites of the same cluster, or proceeding via different TS geometries on the same Pt site. For reference, the ensemble of metastable isomers for the Pt_7 and Pt_8 clusters on γ-Al_2O_3 determined independently by grand canonical basin hoping (minimum) global optimization is provided in Figure S3-S5.
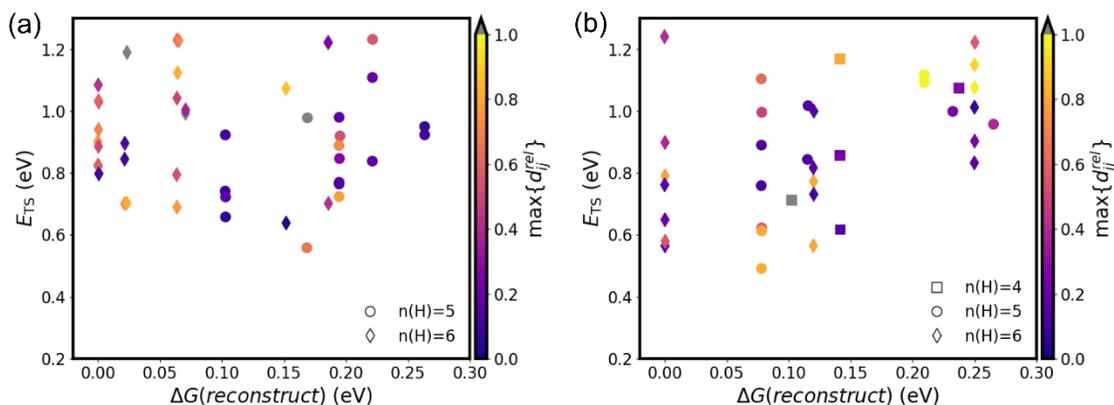

Figure 2: Ensemble of most effective reaction pathways for C-H bond activation of methane. The y axis shows the free energy of the TS (noted as E_{TS}), referenced to the free energy of the global minimum of the supported cluster and gas phase CH_4 and the x axis is the free energy of the EC using the global minimum as reference. (a) Pt_7H_x@γ-Al_2O_3(100), and (b) Pt_8H_x@γ-Al_2O_3(100) surfaces. Conditions are 600°C and 0.1 bar of H_2. The shape of the symbol indicates the number of H co-adsorbates. The geometric deviation between the reactant cluster and the corresponding TS ($\max\{d_{ij}^{rel}\}$) is coded by the color of the symbol.

At the considered (T,P) conditions, between 4 and 6 H atom co-adsorbates (as indicated by the symbol shape) are found with the dissociating methane on the clusters. The structures of the 12 lowest energy TSs and of the corresponding ECs are shown in Figures S9-10. Such a high complexity involved in one reaction step (i.e. the first C-H breaking for an alkane), consisting of contributions from various cluster structures, sites, as well as TS geometries, has not been addressed yet, to our knowledge. Note that all the pathways shown on Figure 2 are verified by optimizing structure following the virtual mode, and that at the end both reactants and products are obtained.

2.2 Cluster reconstruction during reaction: facilitating reaction, as well as creating active sites.

Let us now focus on the changes of cluster geometry between those low energy TSs found by the GAS approach and the corresponding ECs. In order to systematically investigate the reconstructions for the ensemble of pathways, we built two descriptors: the first one (d_{ii}) indicates the displacement of an atom i between the EC in the absence of methane and the same atom in the TS; the second (d_{ij}^{rel}) indicates the change of interatomic distances between atom i and j, normalized by the equilibrium bond length (see detailed explanation in Figure S6). The amplitude of the geometry change (seen as the maximum d_{ii}^{rel} of each channel) is coded by the color of the symbols on Figure 2(a)(b), and importantly, many of accessible TSs deviate significantly from the corresponding EC.

We can underline two types of catalyst reconstruction playing a role in the activity. In the first type, the cluster geometry at the low-energy TS is only slightly modified compared to the EC, and these pathways are indicated by the dark blue symbols in Figure 2(a)(b). The reconstruction of the cluster from the GM to the EC promotes the subsequent reactivity (Figure 1, case TS$_B$). We call this type of reconstruction "independent reconstruction", since it can exist in the absence of CH$_4$ activation. In addition, we found another important type of reconstruction: reaction-induced concomitant cluster reconstruction, which results in a configuration of the cluster distinct, in geometry and electronic structure, from any metastable isomer of the supported cluster (shown in orange and yellow labels in Figure 2(a)(b)). In the latter case, the geometry of the cluster in the TS is not a local minimum in the absence of reactants, and can only appear in the course of the reactive trajectory (Figure 1, case TS$_C$).

Exploring in more details the 12 lowest energy pathways for Pt$_7$ or Pt$_8$ clusters we see that, for the majority of them, important concomitant reconstructions are seen between reactant cluster and TSs, with displacement of atoms by more than 1 Å, and change of interatomic distance of 50 % or more, showing bond breaking or bond-formation (Figure 3 (a),(b) and Figure S6-8). This clearly indicates that the most active site in reaction conditions presents concomitant reconstruction as an essential mechanism for boosting the activity. This rearrangement is not major for Pt-Pt bonds, but the large $d_{ij}^{rel} > 0.5$ (Pt-H) clearly demonstrates significant H migrations during cluster deformation, and the large d_{ij}^{rel} of Pt-Al or Pt-O bonds shows that the modification of the cluster-

oxide interaction is also responsible for creating highly active Pt sites, for example by detachment of some cluster Pt atoms from the support (Figures S7 and S8). Therefore, catalyst reorganization is an essential part of the reaction coordinate, which is not systematically considered in standard models of heterogeneous catalysis.
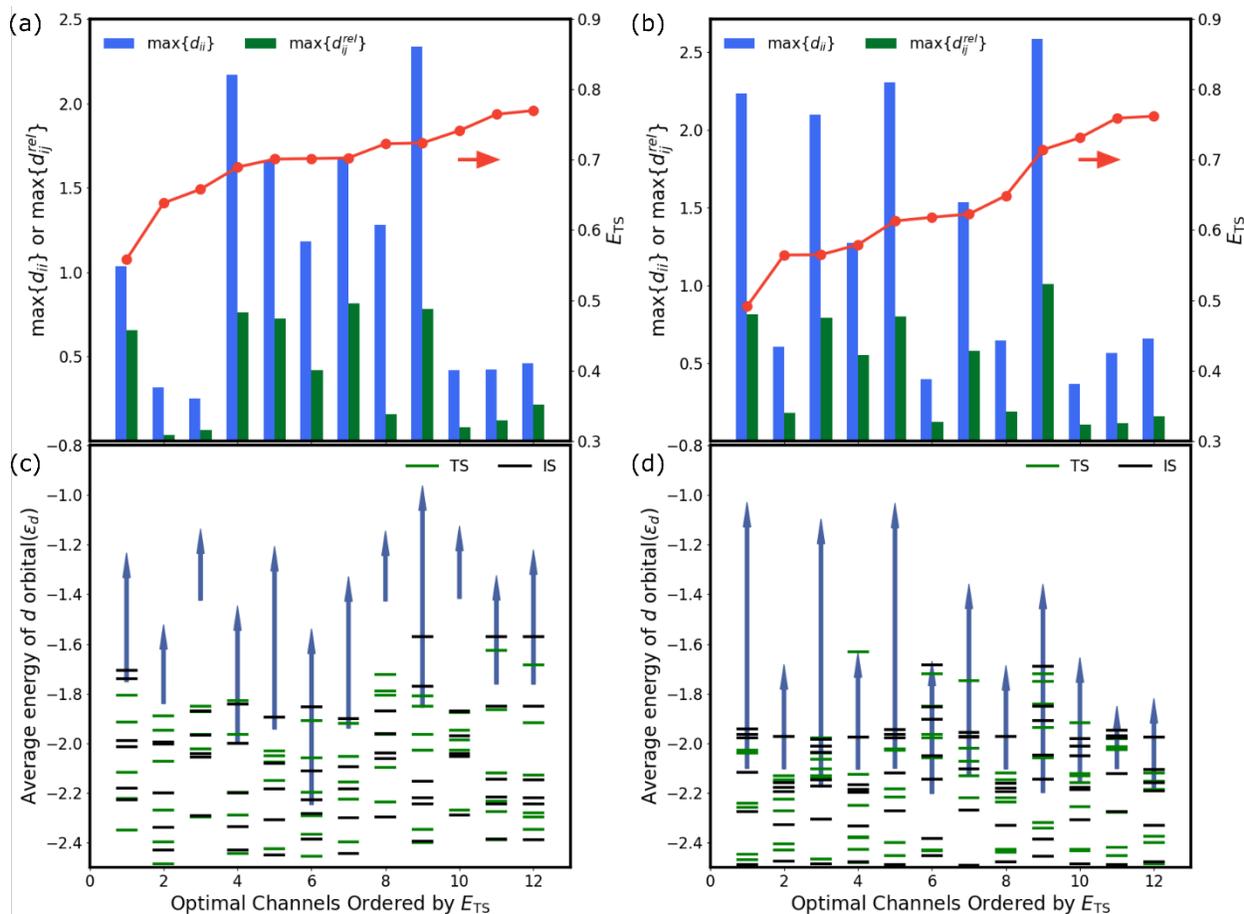

Figure 3: Concomitant reconstruction of the cluster is often required to create the active site. (a) and (b): maximum atomic displacement $\max(d_{ii})$ (blue bars, Å) or changes of interatomic distances normalized by covalent radii max (d_{ij}^{rel}) (green bars, no unit) between the metastable cluster isomer and the TS configurations for the first 12 most active reaction channels on Pt_7 and Pt_8 cluster respectively. E_{TS} is recalled for each channel (red line, eV, right axis). (c) and (d): electronic consequence of the deformation shown as the shift of the d state mean energy (ε_d) for the active Pt from the metastable isomer to the TS for each channel (light blue arrow, eV). The ε_d for other Pt atoms in the considered metastable cluster isomer are shown by black and green lines, for the metastable isomers and TS geometries respectively.

Figure 4 details for illustration the cases of the first and fourth optimal reaction channel on the Pt_7 and Pt_8 clusters, respectively, since they show large concomitant reconstructions. Figure 4(a) shows the structure of the reactant cluster with formula Pt_7H_5, which is 0.17 eV higher than the

GM (Pt_7H_6). From that point, a further concomitant restructuring of the cluster is required to reach the configuration providing the lowest C-H dissociation transition state:
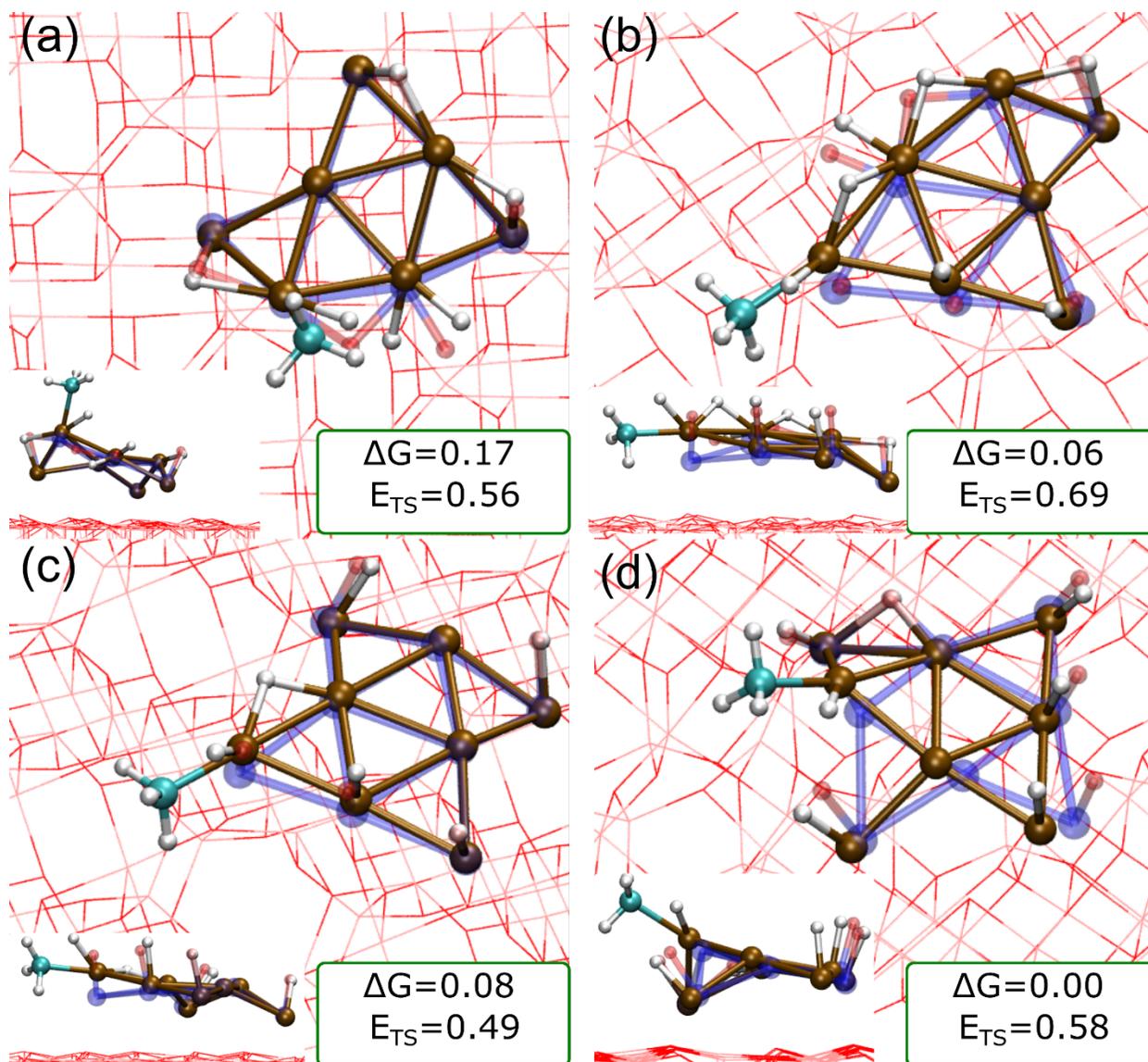

Figure 4: Illustration of the cluster reconstructing during the CH_4 activation. The substrates (Al_2O_3) are shown by red lines to hide the details. Insets are side view for each pathway to illustrate the detachment of Pt from surface (mainly for (b)(c)). The reactant clusters are shown by half transparent balls in which hydrogen is pink and platinum is blue. The TSs are shown by solid balls in which platinum is brown, hydrogen is white and carbon is green. *(a), (b)* are the first and fourth optimal channels on Pt_7 cluster, and (c),(d) are the first and fourth optimal channels for Pt_8 cluster. The free energy of the reactant cluster with respect to GM (ΔG) and the energy of the TS (E_{TS}) are shown in the lower right corners.

the neighboring H migrates from a bridge site to a top site in which one of the Pt-H distances changes from 1.73 to 2.83 Å (d_{ii}= 1.035 Å, $d_{ij}^{rel} = 0.66$ see also Figure 3). The reconstruction is even more significant in the case of the optimal channel of the Pt_8 cluster. Figure 4(c) shows that the Pt_8H_5 cluster, in the metastable geometry 0.08 eV above the GM, originally lies flat on the γ-

9

Al$_2$O$_3$(100) surface and has five top site hydrogen atoms. In the configuration associated with the highest C-H dissociation activity, the Pt atom involved in the interaction with the methane is lifted up by 0.9 Å and uncoordinated from the support, while the H atom on it leans towards the neighboring bridge site, forming a new Pt-H bond. Finally, the ensemble of reaction pathways shows various other mechanisms for concomitant reconstruction. The second optimal pathways of both clusters are characterized by a very weak deformation from the EC cluster to the TS (Figure 3(a,c)). In contrast, the pathways shown in Figure 4(b,d) again show strong concomitant reconstruction, by breaking Pt-support bonds (Figure 4(b)), or even the collective motion of the whole clusters (Figure 4(d)). Before reaching the rate-determining TS, the interaction between methane and the reactant clusters may result in a shallow minimum in the energy profile, but will not influence the rate-determining step shown in Figure 4 (Section S5 and Figure S12). The detachment of the Pt site atom from the support, concomitantly with the C-H bond dissociation is therefore an important mode of restructuring for high activity. Such movements can be controlled by the strength of the metal-support interaction.

These cluster configurations at TS, involving migrated H atoms or Pt atoms detached from the support, only exist at the TS for C-H bond dissociation, and are not local minima in the absence of the reactant. If methane is removed, they return to the corresponding ECs, i.e. the reactant state. Hence, a deformation of the cluster in a transient geometry concomitant with the approach of methane is required to reach an optimal active site for C-H bond breaking. The same Pt atom in the EC structure, occupied by a H atom or stabilized by interaction with the support, is unable to activate CH$_4$ without restructuring. To further support the critical role of using the GAS approach in uncovering the concomitant reconstruction, we followed a manual approach and attached the activated reactant (i.e. CH$_4$ with elongated C-H bond) on the metastable structures of the clusters to explore C-H dissociation TSs. The produced TSs are close to the original geometry of the reactant cluster and at least 0.26 eV higher in energy than the TSs obtained with GAS (Supporting information section S4 and Figure S11). Specifically, the detachment of the Pt atom from the support and the migration of the H atom, key for the low energy channel, are not seen. The *potential energy surface* of the cluster (implicitly constrained at CH$_4$ as transition state structure) is complex, presenting several minima, some of the local minima being close to the reactant state configuration, while others, more distant, can provide lower TS energies (Figure 1 TS$_c$). This shows that explicit sampling of cluster configuration at the C-H dissociation transition state is

required to reach the best catalytic channel, while only sampling configurations for the EC in absence of methane followed by pathway searches is insufficient.

We should note that, in analogy of any global optimization methods, the strength of GAS is the automation based on just minimal prior knowledge (such as the topology of the C-H dissociation TS on Pt), and then the automation has the potential to produce novel results in a systematic way. Altogether, our approach opens the way to the explicit sampling of activity space for dynamic catalysts.

Unlike the scenario on static extended surfaces, where the energies of TSs can be estimated by knowing only the electronic structure or coordination number of the catalytic site in the absence of reaction,[45-47] it is non-trivial to predict the optimal restructuring and corresponding TS energy using only the electronic structure of the reactant cluster. The reconstructions that create highly active sites produces a combination of geometric and electronic effects. The metastable isomer of Pt_8 (Figure 4(c)) presents a flat geometry on γ-Al_2O_3(100), and, although there are two Pt sites (in the center of the cluster) that seem available for C-H bond activation, their average Pt d state energy (ε_d) are as low as -1.9 eV making them inactive (Figure 3(d) first channel). The edge Pt is already occupied by H and also presents a low ε_d, and thus does not seem to be a preferable site at first sight. However, upon restructuring, as seen above, this Pt atom is lifted up and the H atom moves to the bridge site, vacating the Pt site, and shifting its ϵ_d up by more than 1 eV, rendering it highly active toward methane. This reconstruction specifically activates (i.e. destabilizes) one Pt atom on the cluster, and affects other Pt atoms much less. This role of the reconstruction to activate the Pt active site is general as seen by the black arrows on Figure 3(c-d). In some cases (e.g. on channel 3 on Pt_7, Figure 4(b)), ϵ_d is already high on the metastable isomer, and further deformation from its structure is small.

2.3 Reaction rates from ensemble of pathways

A reaction rate can be calculated for each reaction channel from Figure 2 (a) and (b) by the transition state theory, and these rates can be then weighted by the relative population of each metastable cluster isomer at $T = 600\,°C$ (Figure 5 (a) and (b)). The total rate normalization per one Pt atom is obtained by assuming that channels are independent. Clearly the catalytic rate is not governed by a single reaction channel. In contrast, we found 16 (resp. 10) distinct reaction channels, initiated at 8 (resp.4) distinct cluster isomers, such that each channel contributes 1% or

more to the total rate on Pt_7 (resp. Pt_8). The dominant channel on the 7th configuration (resp. 2nd) for Pt_7 (resp. Pt_8) only represents 33 % (resp. 32 %) of the activity, and therefore, an ensemble of
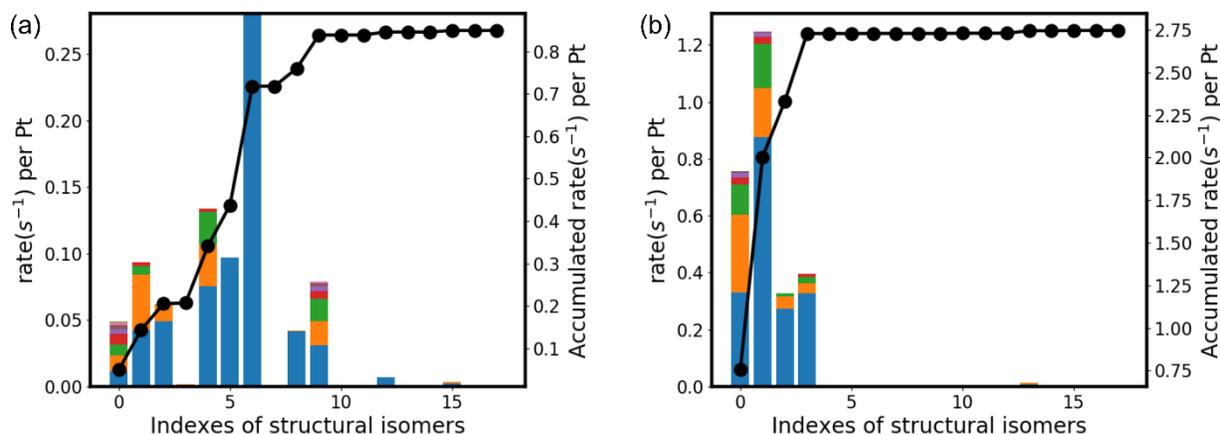

Figure 5 Contribution of each catalyst isomer in the observed C-H bond dissociation reaction rate and cumulative rate, normalized per Pt atom for (a) $Pt_7H_x@\gamma-Al_2O_3(100)$ and (b) $Pt_8H_x@\gamma-Al_2O_3(100)$. Different reaction channels may come from same cluster but on different sites or possessing different TS geometries and they are distinguished by colors.

pathways is required to represent the global kinetics. Any single pathway, even the optimal one is not representative. The GM is only a minor contributor to the total rate (6 % and 28 % on Pt_7 and Pt_8 respectively). The distribution of active channels is different for the two clusters, despite the difference in size by only one atom, with significant activity up to the 9th isomer for Pt_7, and a smaller density of active isomers for Pt_8. However, channels on Pt_8 are more active than those on Pt_7. The total rate is about 3.0 s^{-1} per Pt atom, a value similar to previous experimental measurements.[48] This comparison assumes, as shown previously, that the first C-H dissociation is rate limiting in the dehydrogenation mechanism .[48] In contrast, the standard approach to consider only the GM for the catalytic activity, would give a rate markedly smaller than the experimental value.

If $d_{ij}^{refl} > 0.5$ is used as a criterion to determine the 'contribution' of the concomitant restructuring in the overall rate, the final evaluated contribution of concomitant restructuring is 59% (resp. 69%) for Pt_7 (resp. Pt_8) combing the data from Figure 2 and Figure 5. This implies that without proper sampling of the cluster configuration during exploring the TSs, the total rate will be severely underestimated.

In addition, this calculated rate for alkane C-H dissociation provides a validation for the hypothesis of equilibrium between Pt_nH_x isomers during the catalytic reaction. If cluster isomerization is 100

times faster than C-H bond dissociation rate, then different clusters can safely be considered in equilibrium. The estimated upper bound isomerization barrier for that criterion is as large as 1.9 eV, using a standard prefactor. This large upper bound barrier, compared to the much smaller barriers for the isomerization of similar supported Pt clusters[30], supports the idea of easily reached equilibrium between cluster isomers before reactive events.

3 Conclusion

Catalytic reactivity of supported clusters is generally explained using a static picture for the active site, by electronic and/or steric considerations on a structure, which is a local energy minimum for the catalyst. In this manuscript we show, on the example of C-H bond dissociation on Pt_7 and Pt_8 supported clusters and by an explicit sampling of cluster configurations at C-H dissociation TS, that important change in the structure of the catalyst can be required to reach the most accessible transition state, and, thus, to achieve the optimal activity. This capability of the cluster to reconstruct, simultaneously with the C-H dissociation, is a key aspect explaining its catalytic activity. Hence, the reaction coordinate for the C-H dissociation catalytic event includes degrees of freedom of the cluster catalyst and explicit sampling of these degrees of freedom at the transition state is required to uncover the most favorable pathway. In the absence of the methane reactant, the Pt_7 and Pt_8 clusters on alumina can visit several low energy minima on the potential energy surface. However, in many cases, these metastable configurations of the H covered cluster are not the true active sites. They need to further restructure as the reaction progresses, coupling to the C-H bond dissociation and facilitating it. The concomitant reconstruction of the cluster catalysts mainly involves hydrogen migration and de-coordination of the Pt atoms from the alumina support, rather than the reorganization of the Pt skeleton itself. These changes of structure for the cluster are not unique upon the approach of methane to the Pt site, and standard reaction pathway searches find less favorable transition states with only weak restructuring of the cluster, underlining the importance of an explicit consideration of cluster degrees of freedom in pathway exploration. These structural deformations enhance the activity through combined steric and electronic effects, with strong shifts of the d state mean energy. The restructured cluster configurations providing low TS for C-H dissociation, and involving H atom migration or reorganization of the cluster-support interaction, only exist along the pathway of CH_4 approach and dissociation, and are not local minima in the absence of the reactant. Hence, the equilibrium (metastable) geometries of

supported clusters do not clearly possess the essentials of catalytic activities, and instead the capability of a cluster to deform synergistically with reaction is critical to catalysis.

The proposed GAS method enables a systematic exploration of reaction pathways on fluxional supported cluster catalysts, in an unbiased way, meaning that it uncovers a true reaction coordinate beyond the C-H stretch for methane dissociation. The grand canonical component is important to realistically include reaction conditions, i.e. hydrogen pressure and temperature. For the studied cases of Pt_7 and Pt_8 on γ-Al_2O_3, a large ensemble of reaction channels contributes to the total rate. No single pathway dominates the rate, so that the ensemble description of cluster configurations appears crucial to model and explain the catalytic activity. The global minimum structure generates reactive channels, but their contribution to the total rate is minor, while channels initiated at low energy metastable cluster configurations dominate the catalytic activity.

While obtained on small supported cluster, the qualitative aspects of the results have strong implications for our general understanding of elementary steps and activity in heterogeneous catalysts. Indeed, larger particle catalysts and even model extended surfaces have been shown to provide extensive restructuring in reaction conditions. [1, 49-50] This implies strong mobility of surface atoms of the catalyst and the probable need to sample catalyst degrees of freedom during molecular reaction processes to find optimal pathways and realistically model the catalytic activity and selectivity.

# 4 Methods

4.1 Computational details

GAS explorations are conducted by an in-house package (see SI Section 1) , which is coded on the platform of the ASE package.[51] Energy and forces are calculated by plane waves based density functional theory (DFT) calculations using the Projector augmented wave (PAW) method implemented in The Vienna Ab initio simulation package (VASP).[52-57] The energy cutoff for the plane waves is 400 eV and the Perdew-Burke-Ernzerhof (PBE) functional is used for describing the electron exchange-correlation energies. Spin-polarized calculations are used for all the cases. Only one gamma-point centered k-mesh is used for Brillouin zone sampling.

The γ-Al_2O_3 (100) surface is created according to the bulk γ-Al_2O_3 model proposed by Digne et al.,[58] the formula of the slab model is $Al_{96}O_{144}$, and the dimension of the simulation box is 16.761

Å × 16.826 Å. The bottom half of the slab is always kept as frozen. Local optimization and transition state optimizations are carried by ASE optimizer BFGS, or DIMER method respectively, until the maximum force residue on the atoms is smaller than 0.03 eV/ Å. A Vibrational analysis is performed to confirm that the TSs only show one imaginary frequency and local minima contain no imaginary frequency.

4.2 Reaction rate of light alkane activation on Pt cluster

The reaction starts with gas phase alkane adsorption forming a weakly bound species[59-61] following Langmuir–Hinshelwood kinetics:

$$\text{alkane (gas)} + * \rightarrow \text{alkane(ads)} \tag{1}$$
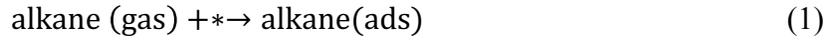
The adsorbed "alkane(ads)" needs to overcome a barrier to form the product, this is the rate determining step of the alkane dehydrogenation:

$$\text{alkane(ads)} \rightarrow \text{product} \tag{2}$$

The rate constant for the reaction (2) can be evaluated by equation (3) using transition state theory:

$$k = \frac{k_B T}{h} e^{\left(-\frac{\Delta G^{\neq}}{k_B T}\right)} = \frac{k_B T}{h} e^{\frac{\Delta S^{\neq}}{k_B}} e^{\left(-\frac{\Delta H^{\neq}}{k_B T}\right)} \tag{3}$$

In equation (3), the $\Delta S^{\neq}$, $\Delta H^{\neq}$ are the activation entropy and activation enthalpy respectively. However, it is known that saturated alkane is only weakly bound to the catalyst, hence the coverage of alkane(ads) is limiting the total reaction rate. Considering the Langmuir adsorption model, the total activation rate should be:

$$
\begin{aligned}
r = \theta_{alkane} k &= \frac{K_{eq} \frac{p^{alkane}}{p^o}}{1 + K_{eq} \frac{p^{alkane}}{p^o}} \frac{k_B T}{h} e^{\frac{\Delta S^{\neq}}{k_B}} e^{\left(-\frac{\Delta H^{\neq}}{k_B T}\right)} \\
&= K_{eq} \frac{p^{alkane}}{p^o} \frac{k_B T}{h} e^{\frac{\Delta S^{\neq}}{k_B}} e^{\left(-\frac{\Delta H^{\neq}}{k_B T}\right)} \\
&= \frac{k_B T}{h} \frac{p^{alkane}}{p^o} e^{\frac{\Delta S^{\neq} + \Delta S_{ads}^o}{k_B}} e^{\left(-\frac{\Delta H^{\neq} + \Delta H_{ads}^o}{k_B T}\right)} \\
&= \frac{k_B T}{h} e^{\frac{\Delta S^{\neq} + \Delta S_{ads}}{k_B}} e^{\left(-\frac{\Delta H^{\neq} + \Delta H_{ads}^o}{k_B T}\right)}
\end{aligned} \tag{4}
$$

In equation (4), p^{alkane} is the partial pressure of the alkane and K_{eq} is the adsorption constant. ΔS_{ads}^o and ΔH_{ads}^o are standard adsorption entropies and enthalpy. We assume $1 \gg K_{eq} \frac{p^{\text{alkane}}}{p^o}$. $\frac{p^{\text{alkane}}}{p^o}$ is adsorbed into ΔS_{ads}. Because the adsorption of alkane lost the translational entropy which dominates the entropy change, hence $\Delta S_{ads} + \Delta S^{\neq} \approx \Delta S_{ads}$. The enthalpy term $\Delta H^{\neq} + \Delta H_{ads}^o$ equals the enthalpy difference between the transition state and the gas phase alkane: H_{TS}-$H_{\text{alkane(gas)}}$. Therefore, the weak adsorption enthalpy does not appear in the effective activation enthalpy.

4.3 The optimization objective

The GAS globally optimizes the TS structure which considers both the stability of entry cluster (EC) and activity of them. To derive the optimization objective, we evaluate the free energy of the EC cluster as G[EC]:

$$G[EC] = E[\text{EC}] - \sum_{j=1}^{N} \mu_j N_j \tag{5}$$

In which, $E[\text{EC}]$ is the electronic energy computed by DFT; μ_j and N_j are the chemical potential and number of atoms for species j in the EC model. The relative occurrence probability of the EC isomer can be estimated by:

$$p[EC] = \exp\left(-\frac{G1}{k_B T}\right) \tag{6}$$

We did not normalize $p[EC]$ in equation (6) yet, but only the relative $p[EC]$ is important for the sampling.

Only hydrogen is in equilibrium with a reservoir at a temperature T and pressure P_{H_2}, and the chemical potential of hydrogen is calculated as following:[29, 62]

$$\mu_H^{T,P_{H_2}} = \frac{1}{2}\left(\mu_{H_2}^{0K} - h_{H_2}^{0K} + k_B T ln\left(\frac{P_{H_2}}{P^\Theta}\right)\right) \tag{7}$$

$h_{H_2}^{0K}$ is the enthalpy of hydrogen at 0 K.

Consider a reaction pathway which starts from EC with barrier as $E_a = \Delta H^{\neq} + \Delta H_{ads}$ (see section 4.3), which is evaluated by:

$$E_a = E(\text{TS}) - E[\text{EC}] - E(\text{CH}_4) \qquad (8)$$

E(TS), E(CH$_4$) are the electronic energies of TS and CH$_4$. Taking the population of the EC cluster into account, the relative contribution of the specific pathway is hence evaluated as:

$$r_{eff} = \text{p(EC)} \times \text{r}$$

$$= \exp\left(-\frac{E[\text{EC}] - \sum_{j=1}^{N} \mu_j N_j}{k_B T}\right)$$

$$\times \frac{k_B T}{h} e^{\frac{\Delta S_{ads}}{k_B}} exp\left(-\frac{E(\text{TS}) - E[\text{EC}] - E(\text{CH}_4)}{k_B T}\right)$$

$$= \frac{k_B T}{h} e^{\frac{\Delta S_{ads}}{k_B}} exp\left(-\frac{E(\text{TS}) - E(\text{CH}_4) - \sum_{j=1}^{N} \mu_j N_j}{k_B T}\right) \qquad (9)$$

$$= \frac{k_B T}{h} e^{\frac{\Delta S_{ads}}{k_B}} exp\left(-\frac{E_{TS}}{k_B T}\right)$$

In which the E_{TS} is defined as

$$E_{TS} = E(TS) - E(CH_4) - \sum_{j=1}^{N} \mu_j N_j \qquad (10)$$

In Equation (10), the N_j (the number of atoms for element j) is calculated as if in the absence of reactant CH$_4$. In the end, GAS sampling optimizes E_{TS} which takes both the stability of EC cluster and activity of alkane into account providing the largest effective reaction rate.

5 Supporting information

Flowchart of GAS, models of γ-Al$_2$O$_3$(100) surface, structures of low free energy clusters and TSs, illustration of notations for d_{ii} and d_{ij}^{ref} comparison between clusters and TSs, precursor structures before C-H activation; geometry coordinates of optimal TS and reactant cluster configurations.

6 Acknowledgements

7 References

1. Tao, F.; Dag, S.; Wang, L. W.; Liu, Z.; Butcher, D. R.; Bluhm, H.; Salmeron, M.; Somorjai, G. A., Break-up of stepped platinum catalyst surfaces by high CO coverage. *Science* **2010**, *327*, 850-3.
2. Weng, Z., et al., Active sites of copper-complex catalytic materials for electrochemical carbon dioxide reduction. *Nat. Commun.* **2018**, *9*, 415.
3. Tao, F.; Crozier, P. A., Atomic-Scale Observations of Catalyst Structures under Reaction Conditions and during Catalysis. *Chem. Rev.* **2016**, *116*, 3487-3539.
4. Zugic, B.; Wang, L.; Heine, C.; Zakharov, D. N.; Lechner, B. A. J.; Stach, E. A.; Biener, J.; Salmeron, M.; Madix, R. J.; Friend, C. M., Dynamic restructuring drives catalytic activity on nanoporous gold-silver alloy catalysts. *Nat. Mater.* **2017**, *16*, 558-564.
5. Sun, G.; Sautet, P., Metastable Structures in Cluster Catalysis from First-Principles: Structural Ensemble in Reaction Conditions and Metastability Triggered Reactivity. *J. Am. Chem. Soc.* **2018**, *140*, 2812-2820.
6. Zhang, Z.; Zandkarimi, B.; Alexandrova, A. N., Ensembles of Metastable States Govern Heterogeneous Catalysis on Dynamic Interfaces. *Acc. Chem. Res.* **2020**, *53*, 447-458.
7. Zhang, Z.; Jimenez-Izal, E.; Hermans, I.; Alexandrova, A. N., Dynamic Phase Diagram of Catalytic Surface of Hexagonal Boron Nitride under Conditions of Oxidative Dehydrogenation of Propane. *J. Phys. Chem. Lett.* **2019**, *10*, 20-25.
8. Hakkinen, H.; Abbet, S.; Sanchez, A.; Heiz, U.; Landman, U., Structural, electronic, and impurity-doping effects in nanoscale chemistry: supported gold nanoclusters. *Angew. Chem. Int. Ed. Engl.* **2003**, *42*, 1297-300.
9. Vajda, S., et al., Subnanometre platinum clusters as highly active and selective catalysts for the oxidative dehydrogenation of propane. *Nat. Mater.* **2009**, *8*, 213-6.
10. Raybaud, P.; Chizallet, C.; Mager-Maury, C.; Digne, M.; Toulhoat, H.; Sautet, P., From γ-alumina to supported platinum nanoclusters in reforming conditions: 10 years of DFT modeling and beyond. *J. Catal.* **2013**, *308*, 328-340.
11. Ferrando, R.; Jellinek, J.; Johnston, R. L., Nanoalloys: From theory to applications of alloy clusters and nanoparticles. *Chem. Rev.* **2008**, *108*, 845-910.
12. Li, G.; Jin, R. C., Atomically Precise Gold Nanoclusters as New Model Catalysts. *Acc. Chem. Res.* **2013**, *46*, 1749-1758.
13. Schmid, G.; Baumle, M.; Geerkens, M.; Helm, I.; Osemann, C.; Sawitowski, T., Current and future applications of nanoclusters. *Chem. Soc. Rev.* **1999**, *28*, 179-185.
14. Scholten, J. D.; Leal, B. C.; Dupont, J., Transition Metal Nanoparticle Catalysis in Ionic Liquids. *ACS Catal.* **2012**, *2*, 184-200.
15. Yan, N.; Xiao, C. X.; Kou, Y., Transition metal nanoparticle catalysis in green solvents. *Coord. Chem. Rev.* **2010**, *254*, 1179-1218.
16. Liu, L.; Corma, A., Metal Catalysts for Heterogeneous Catalysis: From Single Atoms to Nanoclusters and Nanoparticles. *Chem. Rev.* **2018**, *118*, 4981-5079.
17. Cheng, L., et al., Reaction Mechanism for Direct Propylene Epoxidation by Alumina-Supported Silver Aggregates: The Role of the Particle/Support Interface. *ACS Catal.* **2013**, *4*, 32-39.
18. Tyo, E. C.; Vajda, S., Catalysis by clusters with precise numbers of atoms. *Nat. Nanotechnol.* **2015**, *10*, 577.
19. Vajda, S., et al., Subnanometre platinum clusters as highly active and selective catalysts for the oxidative dehydrogenation of propane. *Nature Materials* **2009**, *8*, 213.
20. Valden, M.; Pak, S.; Lai, X.; Goodman, D. W., Structure sensitivity of CO oxidation over model Au/TiO22 catalysts. *Catal. Lett.* **1998**, *56*, 7-10.
21. C. D. Chang; R. Prins; J. H. Sinfelt; R. Von Ballmoos; D. H. Harris; J. S. Magee; A. Stuwe; C.-P. Halsig; H. Tschorn; Sie, S. T., Energy-Related Catalysis. In *Handbook of Heterogeneous Catalysis*, G. Ertl; H. Knozinger; Weitkamp, J., Eds. Wiley-VCH Verlag GmbH: Weinheim, Germany, 1997; Vol. 4-5, pp 1998-2017.
22. Vaarkamp, M.; Miller, J. T.; Modica, F. S.; Koningsberger, D. C., On the Relation between Particle Morphology, Structure of the Metal-Support Interface, and Catalytic Properties of Pt/γ-Al₂O₃. *J. Catal.* **1996**, *163*, 294-305.

23.   Kang, J. H.; Menard, L. D.; Nuzzo, R. G.; Frenkel, A. I., Unusual Non-Bulk Properties in Nanoscale Materials: Thermal Metal−Metal Bond Contraction of γ-Alumina-Supported Pt Catalysts. *J. Am. Chem. Soc.* **2006**, *128*, 12068-12069.

24.   Singh, J.; Nelson, R. C.; Vicente, B. C.; Scott, S. L.; van Bokhoven, J. A., Electronic structure of alumina-supported monometallic Pt and bimetallic PtSn catalysts under hydrogen and carbon monoxide environment. *Phys. Chem. Chem. Phys.* **2010**, *12*, 5668-5677.

25.   Wales, D. J.; Doye, J. P. K., Global Optimization by Basin-Hopping and the Lowest Energy Structures of Lennard-Jones Clusters Containing up to 110 Atoms. *J. Phys. Chem. A* **1997**, *101*, 5111-5116.

26.   Yang, Y. I.; Niu, H.; Parrinello, M., Combining Metadynamics and Integrated Tempering Sampling. *J. Phys. Chem. Lett.* **2018**, *9*, 6426-6430.

27.   Zhai, H.; Alexandrova, A. N., Fluxionality of Catalytic Clusters: When It Matters and How to Address It. *ACS Catal.* **2017**, *7*, 1905-1911.

28.   Gao, M.; Lyalin, A.; Takagi, M.; Maeda, S.; Taketsugu, T., Reactivity of Gold Clusters in the Regime of Structural Fluxionality. *J. Phys. Chem. C* **2015**, *119*, 11120-11130.

29.   Sun, G.; Alexandrova, A. N.; Sautet, P., Pt8 cluster on alumina under a pressure of hydrogen: Support-dependent reconstruction from first-principles global optimization. *J. Chem. Phys.* **2019**, *151*, 194703.

30.   Zhai, H.; Alexandrova, A. N., Local Fluxionality of Surface-Deposited Cluster Catalysts: The Case of Pt7 on Al2O3. *J. Phys. Chem. Lett.* **2018**, *9*, 1696-1702.

31.   Guo, H.; Sautet, P.; Alexandrova, A. N., Reagent-Triggered Isomerization of Fluxional Cluster Catalyst via Dynamic Coupling. *J. Phys. Chem. Lett.* **2020**, *11*, 3089-3094.

32.   Artrith, N.; Kolpak, A. M., Grand canonical molecular dynamics simulations of Cu–Au nanoalloys in thermal equilibrium using reactive ANN potentials. *Comp. Matter. Sci.* **2015**, *110*, 20-28.

33.   Calvo, F.; Schebarchov, D.; Wales, D. J., Grand and Semigrand Canonical Basin-Hopping. *J. Chem. Theory Comput.* **2016**, *12*, 902-9.

34.   Revard, B. C.; Tipton, W. W.; Yesypenko, A.; Hennig, R. G., Grand-canonical evolutionary algorithm for the prediction of two-dimensional materials. *Phy. Rev. B* **2016**, *93*.

35.   Tipton, W. W.; Hennig, R. G., A grand canonical genetic algorithm for the prediction of multi-component phase diagrams and testing of empirical potentials. *J. Phys. Condens. Matter.* **2013**, *25*, 495401.

36.   Wexler, R. B.; Qiu, T.; Rappe, A. M., Automatic Prediction of Surface Phase Diagrams Using Ab Initio Grand Canonical Monte Carlo. *J. Phys. Chem. C* **2019**, *123*, 2321-2328.

37.   Hansen, E.; Rosales, A. R.; Tutkowski, B.; Norrby, P.-O.; Wiest, O., Prediction of Stereochemistry using Q2MM. *Acc. Chem. Res.* **2016**, *49*, 996-1005.

38.   Maeda, S.; Ohno, K., Lowest Transition State for the Chirality-Determining Step in Ru((R)-BINAP)-Catalyzed Asymmetric Hydrogenation of Methyl-3-Oxobutanoate. *J. Am. Chem. Soc.* **2008**, *130*, 17228-17229.

39.   Sameera, W. M. C.; Maeda, S.; Morokuma, K., Computational Catalysis Using the Artificial Force Induced Reaction Method. *Acc. Chem. Res.* **2016**, *49*, 763-773.

40.   Zhao, W.; Chizallet, C.; Sautet, P.; Raybaud, P., Dehydrogenation mechanisms of methyl-cyclohexane on γ-Al$_2$O$_3$ supported Pt$_{13}$: Impact of cluster ductility. *J. Catal.* **2019**, *370*, 118-129.

41.   Guo, A. Z.; Sevgen, E.; Sidky, H.; Whitmer, J. K.; Hubbell, J. A.; de Pablo, J. J., Adaptive enhanced sampling by force-biasing using neural networks. *J. Chem. Phys.* **2018**, *148*, 134108.

42.   Sevgen, E.; Giberti, F.; Sidky, H.; Whitmer, J. K.; Galli, G.; Gygi, F.; de Pablo, J. J., Hierarchical Coupling of First-Principles Molecular Dynamics with Advanced Sampling Methods. *J. Chem. Theory Comput.* **2018**, *14*, 2881-2888.

43.   Xu, J.; Huang, H.; Hu, P., An approach to calculate the free energy changes of surface reactions using free energy decomposition on ab initio brute-force molecular dynamics trajectories. *Phys. Chem. Chem. Phys.* **2020**, *22*, 21340-21349.

44.   Martínez-Suárez, L.; Siemer, N.; Frenzel, J.; Marx, D., Reaction Network of Methanol Synthesis over Cu/ZnO Nanocatalysts. *ACS Catal.* **2015**, *5*, 4201-4218.

45.   Bligaard, T.; Nørskov, J. K.; Dahl, S.; Matthiesen, J.; Christensen, C. H.; Sehested, J., The Brønsted–Evans–Polanyi relation and the volcano curve in heterogeneous catalysis. *J. Catal.* **2004**, *224*, 206-217.

46.   Fernández, E. M., et al., Scaling Relationships for Adsorption Energies on Transition Metal Oxide, Sulfide, and Nitride Surfaces. *Angew. Chem. Int. Ed. Engl.* **2008**, *47*, 4683-4686.

47.   Calle-Vallejo, F.; Tymoczko, J.; Colic, V.; Vu, Q. H.; Pohl, M. D.; Morgenstern, K.; Loffreda, D.; Sautet, P.; Schuhmann, W.; Bandarenka, A. S., Finding optimal surface sites on heterogeneous catalysts by counting nearest neighbors. *Science* **2015**, *350*, 185-9.

48.   Sattler, J. J. H. B.; Ruiz-Martinez, J.; Santillan-Jimenez, E.; Weckhuysen, B. M., Catalytic Dehydrogenation of Light Alkanes on Metals and Metal Oxides. *Chem. Rev.* **2014**, *114*, 10613-10653.

49.   Eren, B.; Zherebetskyy, D.; Patera, L. L.; Wu, C. H.; Bluhm, H.; Africh, C.; Wang, L.-W.; Somorjai, G. A.; Salmeron, M., Activation of Cu(111) surface by decomposition into nanoclusters driven by CO adsorption. *Science* **2016**, *351*, 475.

50.   Bergmann, A.; Roldan Cuenya, B., Operando Insights into Nanoparticle Transformations during Catalysis. *ACS Catal.* **2019**, *9*, 10020-10043.

51.   Hjorth Larsen, A., et al., The atomic simulation environment-a Python library for working with atoms. *J. Phys. Condens. Matter.* **2017**, *29*, 273002.

52.   Kresse, G.; Hafner, J., Ab initiomolecular dynamics for liquid metals. *Phys. Rev. B* **1993**, *47*, 558-561.

53.   Kresse, G.; Hafner, J., Ab initiomolecular-dynamics simulation of the liquid-metal–amorphous-semiconductor transition in germanium. *Phys. Rev. B* **1994**, *49*, 14251-14269.

54.   Kresse, G.; Furthmüller, J., Efficiency of ab-initio total energy calculations for metals and semiconductors using a plane-wave basis set. *Comput. Mater. Sci.* **1996**, *6*, 15-50.

55.   Kresse, G.; Furthmüller, J., Efficient iterative schemes forab initiototal-energy calculations using a plane-wave basis set. *Phys. Rev. B* **1996**, *54*, 11169-11186.

56.   Perdew, J. P.; Burke, K.; Ernzerhof, M., Generalized Gradient Approximation Made Simple. *Phys. Rev. Lett.* **1996**, *77*, 3865-3868.

57.   Kresse, G.; Joubert, D., From ultrasoft pseudopotentials to the projector augmented-wave method. *Phys. Rev. B* **1999**, *59*, 1758-1775.

58.   Digne, M.; Sautet, P.; Raybaud, P.; Euzen, P.; Toulhoat, H., Use of DFT to achieve a rational understanding of acid–basic properties of γ-alumina surfaces. *Journal of Catalysis* **2004**, *226*, 54-68.

59.   Zhu, J.; Yang, M.-L.; Yu, Y.; Zhu, Y.-A.; Sui, Z.-J.; Zhou, X.-G.; Holmen, A.; Chen, D., Size-Dependent Reaction Mechanism and Kinetics for Propane Dehydrogenation over Pt Catalysts. *ACS Catalysis* **2015**, *5*, 6310-6319.

60.   Shan, Y. L.; Zhu, Y. A.; Sui, Z. J.; Chen, D.; Zhou, X. G., Insights into the effects of steam on propane dehydrogenation over a Pt/Al2O3 catalyst. *Catalysis Science & Technology* **2015**, *5*, 3991-4000.

61.   Li, Q.; Sui, Z. J.; Zhou, X. G.; Chen, D., Kinetics of propane dehydrogenation over Pt-Sn/Al2O3 catalyst. *Applied Catalysis a-General* **2011**, *398*, 18-26.

62.   Mager-Maury, C.; Bonnard, G.; Chizallet, C.; Sautet, P.; Raybaud, P., H_2-Induced Reconstruction of Supported Pt Clusters: Metal-Support Interaction versus Surface Hydride. *ChemCatChem* **2011**, *3*, 200-207.

TOC graphics
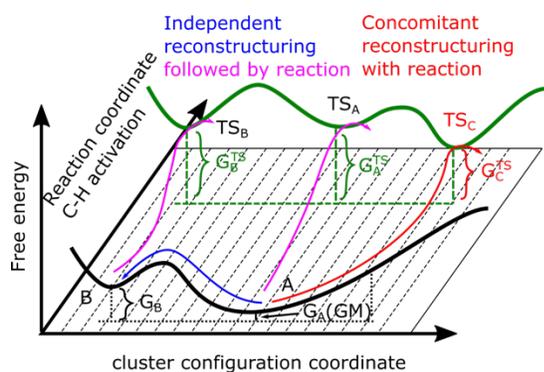
Explicit sampling of the degrees of freedom of the catalytic site in the reaction coordinate is crucial in order to find the catalyst configurations that provide the optimal C-H bond dissociation transition state for alkanes and hence explain the catalytic activity.